Internal report to E89-003 collaboration

Updated Normalization Factors and A_{LT} for ^{16}O$(e, e'p)(1p)^{-1}$ Version 3

James J. Kelly

Department of Physics, University of Maryland, College Park, MD 20742

(Dated: November 10, 2003)

Abstract

In October 1999 I made a survey of the normalization factors needed to fit data for p-shell knockout from ^{16}O obtained in several experiments, expecting that that study would represent one section of a PRC paper to be prepared shortly thereafter. Three years later that paper finally appears to be approaching completion, but the previous calculations are now obsolete. Here I update the previous analysis using similar model input but now using fully relativistic calculations – the effective momentum approximation is no longer needed for spinor distortion. The second significant change is that the normalization factors are obtained by least-squares fitting to data for $|p_m| \leq 200$ MeV/c rather than by eye. Finally, we now consider the NLSH-P wave functions also. This report is a work in progress and will updated several times until the PRC paper is submitted and accepted.

I. OBJECTIVE

The purpose of this work is to evaluate spectroscopic factors for the lowest $1p_{1/2}$ and $1p_{3/2}$ fragments populated by the $^{16}\mathrm{O}(e,e'p)$ reaction. We consider most of the data produced since 1980. RDWIA calculations are performed for the kinematical conditions for each of these experiments and normalization factors determined by least-squares fits to the data for $p_m \leq 200$ MeV/c where the reaction model should be most reliable. When unresolved, the contribution of the $2s1d$ doublet to the $1p_{3/2}$ is included incoherently. Several choices of optical model and bswf are used to form a qualitative estimate of the model dependence of these extractions.

The first version was prepared in October 1999 and several revisions have been made since. Excerpts from this report should appear in a PRC article that has been in preparation for a long time.

Version 1: October 25, 1999
Version 2: December 12, 2002
Version 3: November 10, 2003

II. MODEL

The basic model parameters are summarized in Table I. All of the data were analyzed using the same models. Unless stated otherwise, the calculations are fully relativistic. Distorted waves for the ejectile were obtained using the second-order form of the Dirac equation.

TABLE I: Summary of model input.

bound-state wave function	HS, NLSH, or NLSH-P
optical model	EDAIO or EDAD1
electron distortion	EMA
vertex function	$\bar{\Gamma}_2$
form factors	MMD
gauge	Coulomb

III. DATA BASE

The kinematics of the available data are summarized in Table II and the explanatory remarks below.

- Leuschner: the data were provided and analyzed in the form of reduced cross sections. The $1p_{3/2}$ state was resolved.

- Spaltro: the data were provided and analyzed in the form of differential cross sections. The $1p_{3/2}$ state was resolved. The normalization factors are based upon data for the highest beam energy.
- Chinitz: the data were provided and analyzed in the form of differential cross sections. For the $1p_{3/2}$ state I used data corrected for the positive-parity contamination by the authors.
- Gao: the data were provided and analyzed in the form of differential cross sections. The normalization factors are based upon data for the highest beam energy. The positive-parity contribution to the 6.32 MeV peak was computed using the parametrizations of Leuschner *et al.* and added incoherently to the $1p_{3/2}$ contribution.
- Bernheim: the data were provided and analyzed in the form of reduced cross sections. The positive-parity contribution to the 6.32 MeV peak was computed using the parametrizations of Leuschner *et al.* and added incoherently to the $1p_{3/2}$ contribution.
- Blomqvist: two experiments with rather different kinematics are included; the $1p_{3/2}$ state was resolved. The data were provided and analyzed in the form of reduced cross sections. Calculations were made for each point in these data sets. The kinematics for $T_p \approx 215$ MeV were highly varied.

TABLE II: Summary of kinematical conditions for various experiments.

panel	experiment	type	T_p	Q^2	x
a	Leuschner	$\parallel$	96		
b	Spaltro	$\perp$	84	0.20	1.07
c	Chinitz	$\perp$	160	0.30	0.91
d	Gao	$\perp$	427	0.80	0.96
e	Bernheim	$\perp$	100	0.19	0.90
f	Blomqvist 1	$\parallel$	92	0.08	0.3 – 0.5
g	Blomqvist 2		215	0.04 – 0.26	0.07 – 0.7

IV. NORMALIZATION FACTORS

Fits for four combinations of optical potential and bound-state wave function are shown in Figs. 1-6, where the panels are labeled according to Table II. Normalization factors were deduced from chi-square fits to data for $|p_m| < 200$ MeV/c and are listed in Tables III and IV. Incoherent contributions from the positive-parity contamination of the lowest $1p_{3/2}$ fragment were included in the analysis of data for experiments that did not resolve those contributions. The sd contributions were obtained from the fit shown in Fig. 7 to the Leuschner data for $E_m = 5.3$ MeV. The upper components of the overlap functions were obtained from a Woods-Saxon parametrization and the lower components from the spin-orbit potential; the parameters will be specified later in more detail if needed. The resulting normalization factors, relative to full occupancy, are 0.017 for $2s_{1/2}$ and 0.015 for $1d_{5/2}$.

TABLE III: Normalization factors for lowest $1p_{1/2}$ fragment.

		Normalization factor			χ^2_ν		
experiment	optical model	HS	NLSH	NLSH-P	HS	NLSH	NLSH-P
Leuschner	edaio	0.546	0.597	0.525	0.910	2.465	0.970
Leuschner	edad1	0.597	0.658	0.572	0.784	2.303	0.823
Spaltro	edaio	0.605	0.648	0.581	2.687	5.416	2.318
Spaltro	edad1	0.708	0.766	0.675	2.306	4.208	2.201
Chinitz	edaio	0.537	0.600	0.513	8.680	24.757	8.939
Chinitz	edad1	0.585	0.664	0.559	7.973	16.718	7.172
Gao	edaio	0.618	0.701	0.592	30.841	0.485	19.628
Gao	edad1	0.620	0.704	0.596	32.456	1.229	19.964
Bernheim	edaio	0.428	0.479	0.424	1.004	2.241	0.996
Bernheim	edad1	0.476	0.543	0.468	1.002	1.484	0.958
Blomqvist 1	edaio	0.528	0.540	0.508	3.011	5.044	2.679
Blomqvist 1	edad1	0.569	0.586	0.543	3.239	5.844	2.688
Blomqvist 2	edaio	0.423	0.440	0.404	2.024	4.730	2.491
Blomqvist 2	edad1	0.423	0.440	0.404	1.795	6.604	1.854

A. Sensitivity to bswf

Three relativistic mean field (RMF) models have been considered. The original HS model is the oldest, while the NLSH model was optimized for medium to heavy nuclei. Although NLSH is supposed to be an improvement over the older HS model, light nuclei were not considered and there is no guarantee that it is better for oxygen; hence, the Madrid group fit a variation of the NLSH model, labeled NLSH-P, to the Leuschner data. Plane-wave momentum distributions for these models are compared in Fig. 8. One finds little difference between HS and NLSH wave functions for $1p_{3/2}$ state, but the difference for the ground state is appreciable and the HS model fits most of the low Q^2 data better than the NLSH model. For modest p_m the NLSH-P momentum distribution is close to both NLSH and HS for the $1p_{1/2}$ and is slightly larger near the peak for the $1p_{3/2}$ state, but the NLSH-P momentum distributions for both states fall much faster at large p_m than either the NLSH or HS wave functions. Fits to the Leuschner and Gao data using the EDAIO optical model are compared in Figs. 9-10. Although the NLSH-P model does provide the best fit to the Leuschner data, the momentum densities fall too rapidly to fit the Gao data for large p_m, especially for the $1p_{3/2}$ state. The HS model provides an acceptable fit to the Gao data, but the best fit is obtained with the NLSH model; however, the coverage of the missing momentum distribution is rather sparse. On the other hand, the narrower NLSH-P wave function provides distinctly better fits to most of the low-Q^2 data than either the NLSH or HS models. The NLSH wave functions systematically give the largest normalization factors while the NLSH-P give the smallest; these trends are clearly correlated with the width and heights of the peak of the corresponding momentum distributions.

Therefore, I am inclined to prefer the NLSH-P wave function despite its failure to reproduce the Gao data at large p_m. One could argue that NLSH-P is best at low p_m where RMF

TABLE IV: Normalization factors for lowest $1p_{3/2}$ fragment.

		Normalization factor			χ^2_ν		
experiment	optical model	HS	NLSH	NLSH-P	HS	NLSH	NLSH-P
Leuschner	edaio	0.457	0.466	0.409	4.211	6.028	1.479
Leuschner	edad1	0.549	0.562	0.483	2.424	3.653	1.435
Spaltro	edaio	0.661	0.676	0.577	6.291	7.979	3.642
Spaltro	edad1	0.751	0.770	0.647	5.109	6.355	4.086
Chinitz	edaio	0.559	0.580	0.467	17.850	25.281	14.970
Chinitz	edad1	0.605	0.630	0.500	18.194	22.083	23.807
Gao	edaio	0.628	0.652	0.524	4.686	6.692	15.268
Gao	edad1	0.632	0.655	0.527	2.388	3.868	14.368
Bernheim	edaio	0.457	0.468	0.402	1.899	2.418	1.121
Bernheim	edad1	0.523	0.538	0.453	1.493	1.852	1.252
Blomqvist 1	edaio	0.412	0.415	0.384	4.237	5.790	1.907
Blomqvist 1	edad1	0.500	0.505	0.461	3.673	5.014	2.115
Blomqvist 2	edaio	0.366	0.373	0.325	1.426	1.994	5.918
Blomqvist 2	edad1	0.403	0.410	0.355	1.938	2.769	5.365

should be reliable, but that other effects become important at large p_m, such as correlations, two-body currents, or channel coupling. Although it is generally accepted that short-range correlations tend to deplete the strength of valence states without significantly affecting their p_m distributions, long-range correlations coupled to surface modes may enhance the strength at large p_m. Alternatively, two-body currents are expected to become influential at large p_m even for valence states. Unfortunately, we do not have at this time the calculations needed to distinguish between these possibilities. On the other hand, the continued success of the one-body prediction for A_{LT} over the entire p_m range of the Gao data seems to suggest that the one-body mechanism remains dominant. Of the three models presently available, the HS wave function appears to offer the best compromise (and NLSH the worst) between the low-Q^2 and high-Q^2 data, despite its antiquity, if one is limited to the one-body current.

B. Sensitvity to optical model

Fits to the data show no systematic preference between the EDAD1 or EDAIO optical potentials. However, the dependence of the normalization factors upon the choice of optical model is distressingly large at low Q^2, with EDAIO giving normalization factors that are about 20% smaller at the lowest Q^2 than those from EDAD1. Fortunately, this dependence appears to decrease with Q^2, such that the two potentials are in good agreement by $Q^2 = 0.8$ (GeV/c)^2. Overall, the EDAD1 normalization factors tend to vary less with Q^2. On those grounds one might choose EDAD1 for later figures, rather than continue to use EDAIO. Perhaps a better choice can be found, but the present variation between experiments appears to be too large to remedy by that means. Ordinarily one would expect the higher Q^2 data, namely ours, to be more reliable from the standpoint of the reaction mechanism.

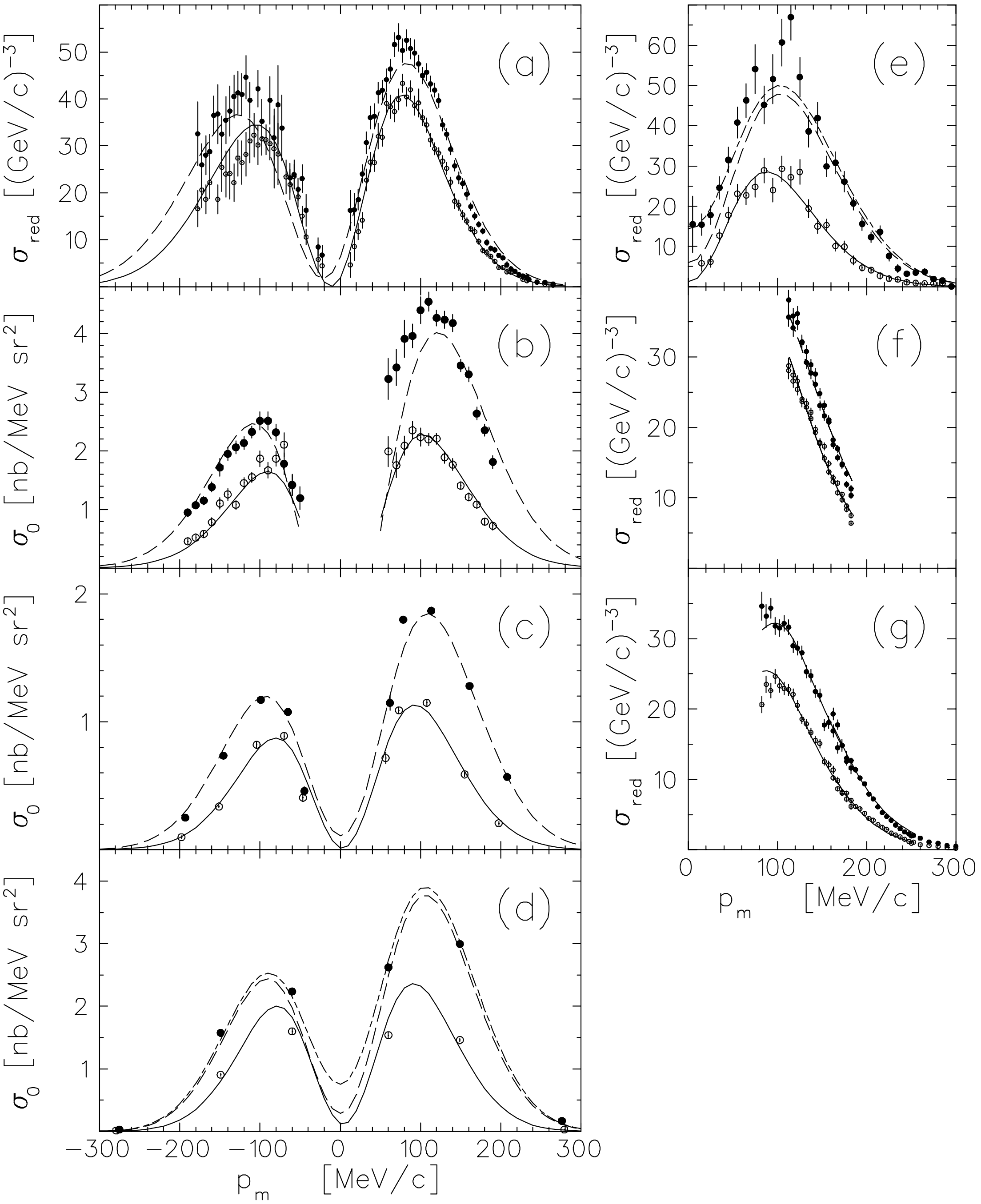

FIG. 1: Scale-factor fits to ^{16}O$(e,e'p)(1p)^{-1}$ data. Open points and solid lines pertain to $1p_{1/2}$, while solid points and dashed lines refer to $1p_{3/2}$. Dash-dotted lines include positive parity contributions to the 6.32 MeV peak. These fits use HS wave functions and the EDAIO optical potential.

C. Proposed text for PRC article

The following is intended to supplement the present draft. [letter] indicates a new reference while [number] refers to an existing reference.

Lapikás *et al.* [a] performed a similar analysis of the Q^2 dependence of spectroscopic

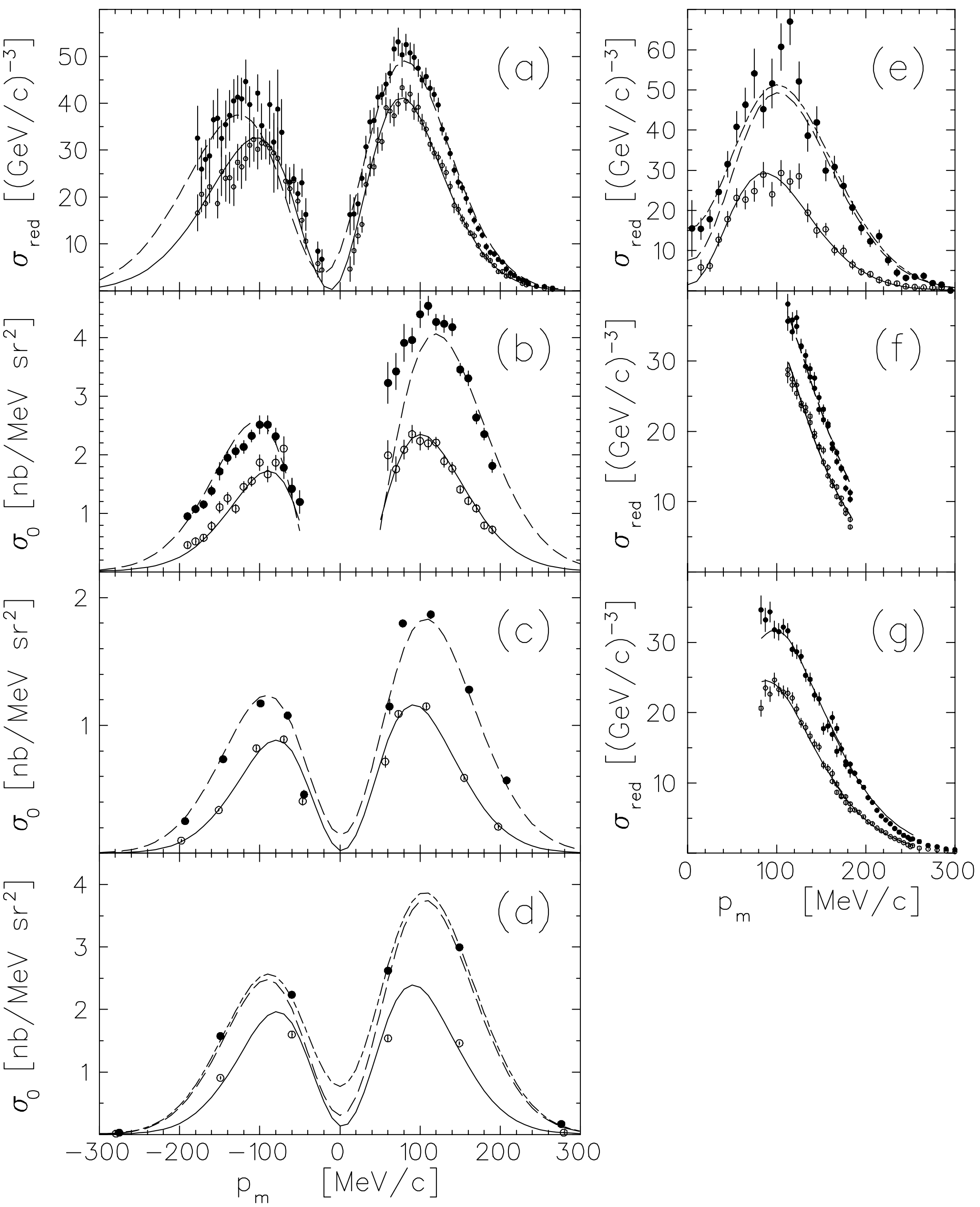

FIG. 2: Scale-factor fits to ^{16}O$(e,e'p)(1p)^{-1}$ data. Open points and solid lines pertain to $1p_{1/2}$, while solid points and dashed lines refer to $1p_{3/2}$. Dash-dotted lines include positive parity contributions to the 6.32 MeV peak. These fits use HS wave functions and the EDAD1 optical potential.

factors for ^{12}C$(e,e'p)^{11}$B. Several data sets with $Q^2 < 0.3$ (GeV/c)^2 were analyzed using a nonrelativistic DWIA model. For each set a normalization factor and the radius parameter for a Woods-Saxon binding potential were fitted to the reduced cross sections for discrete states with the potential depths adjusted to fit the separation energies. Consistent normalization factors were obtained for all data sets except those from Mainz [b]. A new experiment

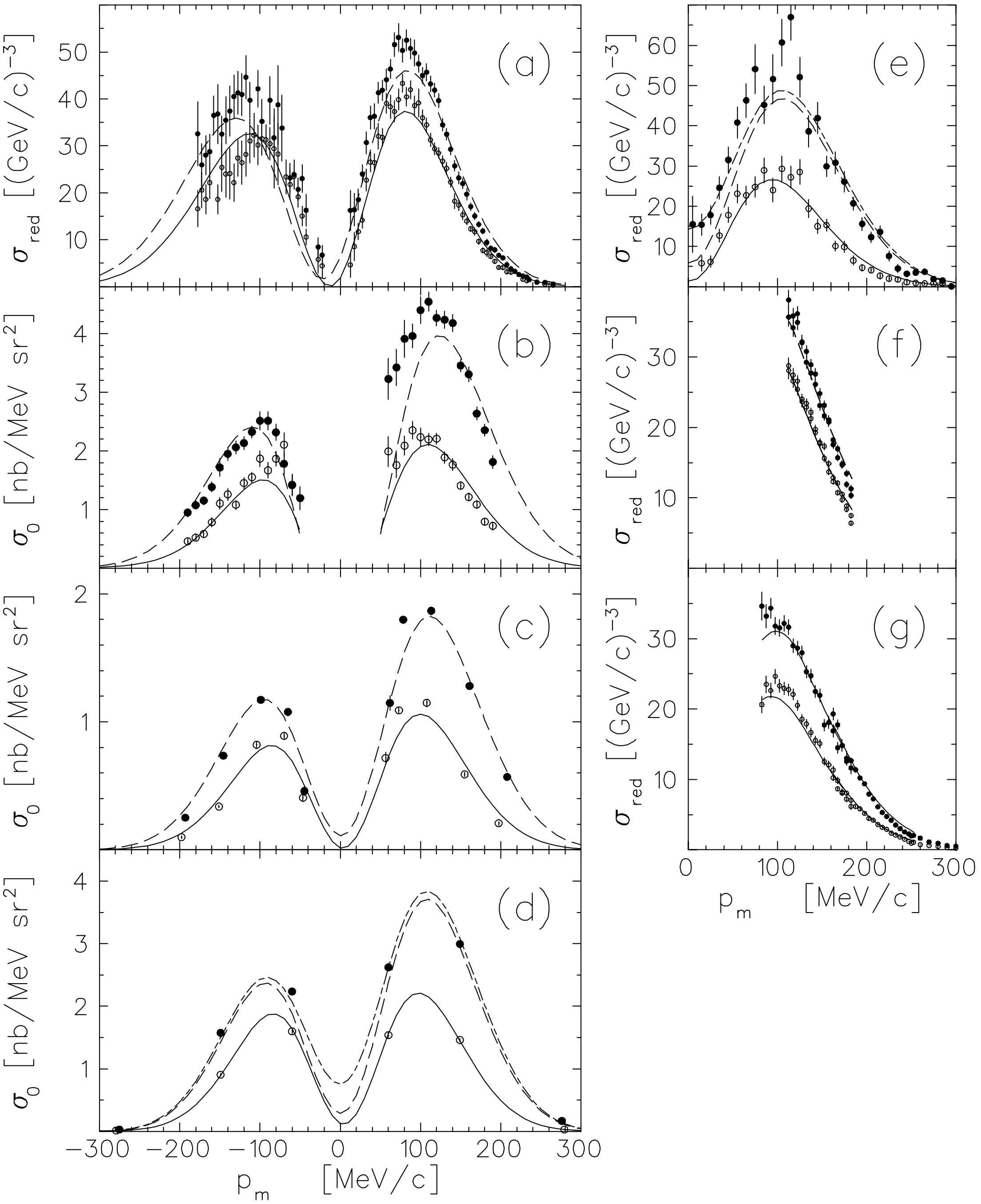

FIG. 3: Scale-factor fits to $^{16}\mathrm{O}(e,e'p)(1p)^{-1}$ data. Open points and solid lines pertain to $1p_{1/2}$, while solid points and dashed lines refer to $1p_{3/2}$. Dash-dotted lines include positive parity contributions to the 6.32 MeV peak. These fits use NLSH wave functions and the EDAIO optical potential.

was performed at NIKHEF duplicating the Mainz kinematics and the new results were also consistent with all data sets except those from Mainz. They concluded that those data were probably normalized incorrectly. Similar doubts about the normalization of the companion experiment [15] on ^{16}O were expressed earlier by Kelly [c] but independent data duplicating those kinematics are not available. Excluding the Mainz data, Lapikás *et al* concluded that

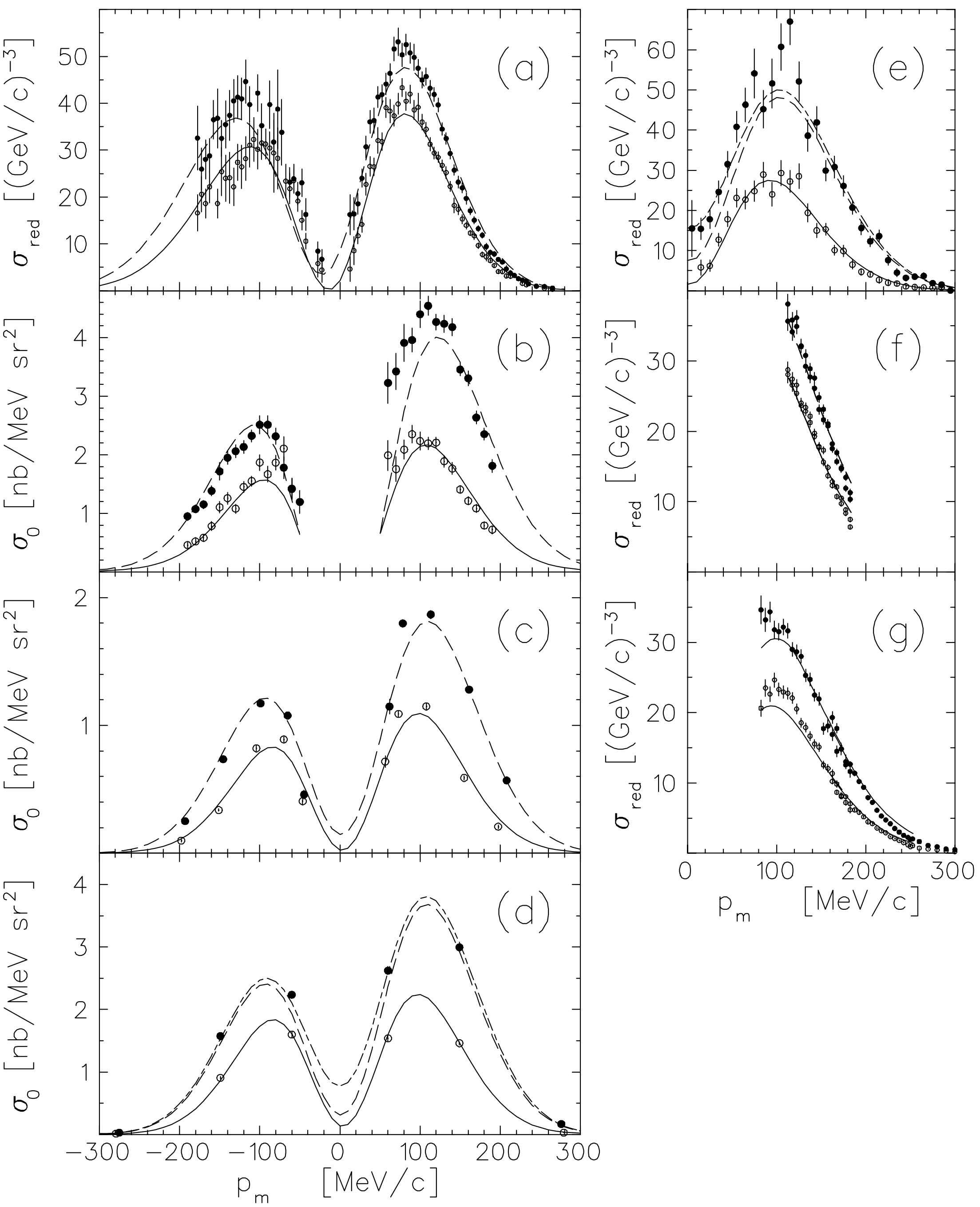

FIG. 4: Scale-factor fits to $^{16}\mathrm{O}(e,e'p)(1p)^{-1}$ data. Open points and solid lines pertain to $1p_{1/2}$, while solid points and dashed lines refer to $1p_{3/2}$. Dash-dotted lines include positive parity contributions to the 6.32 MeV peak. These fits use NLSH wave functions and the EDAD1 optical potential.

the summed $1p$-shell strength for $^{12}\mathrm{C}$ could be deduced from data for $Q^2 < 0.3$ $(\mathrm{GeV}/c)^2$ with an uncertainty of $\pm 3\%$. However, they did not consider variations of the optical model or several other uncertain aspects of the reaction model. Furthermore, it is not clear how much variation of the Woods-Saxon radius might affect the normalization factors. If the overlap function is an intrinsic property of the nuclear wave function, it should not depend

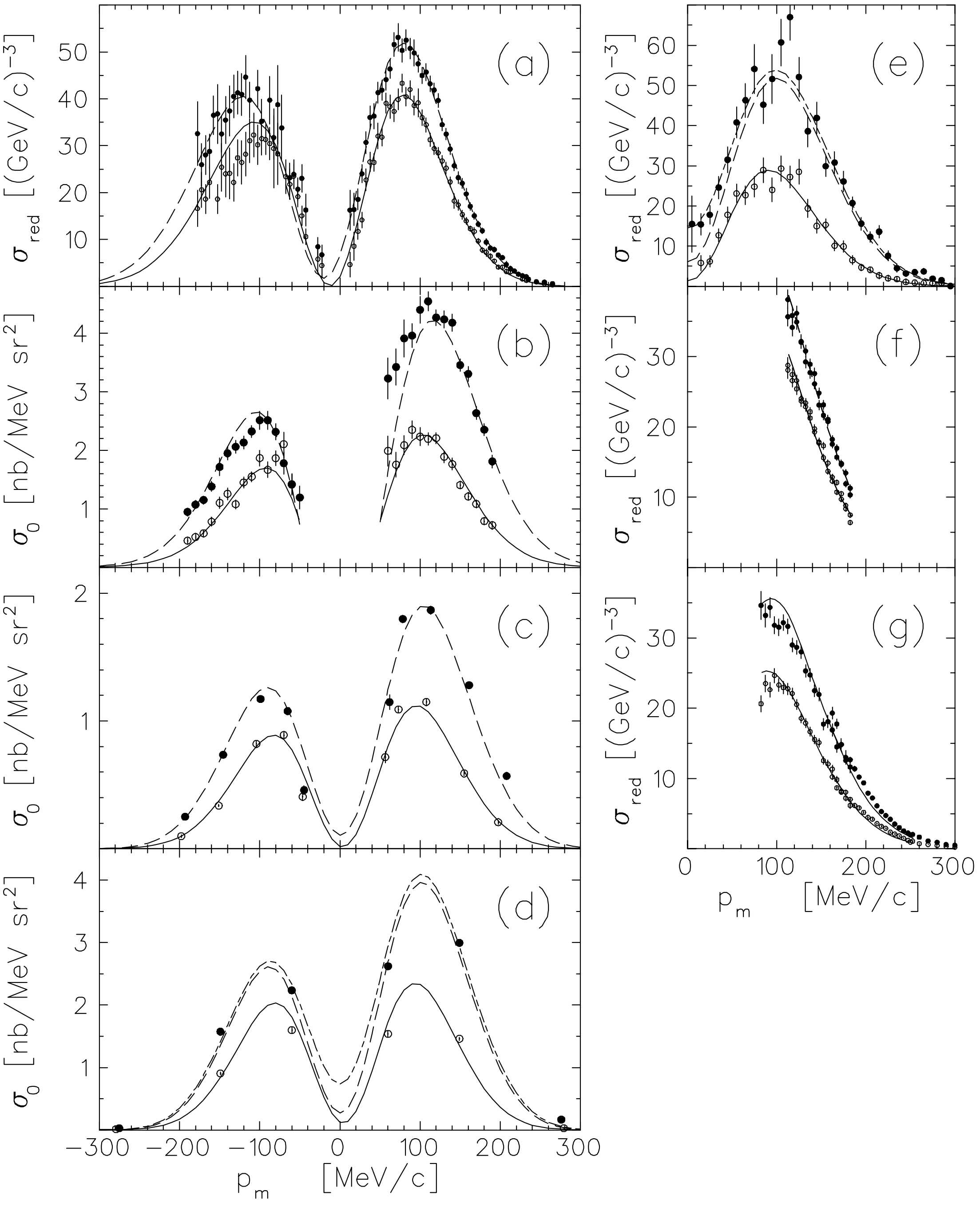

FIG. 5: Scale-factor fits to $^{16}\mathrm{O}(e,e'p)(1p)^{-1}$ data. Open points and solid lines pertain to $1p_{1/2}$, while solid points and dashed lines refer to $1p_{3/2}$. Dash-dotted lines include positive parity contributions to the 6.32 MeV peak. These fits use NLSH-P wave functions and the EDAIO optical potential.

upon Q^2 and it should be possible to fit a common radius to all data simultaneously; if not, one must question the accuracy of the reaction model. Finally, considerable evidence has accumulated in recent years that a relativistic model is preferred not only from general principles but from practical considerations also.

We did not attempt to fit the overlap functions to the knockout data directly, but instead

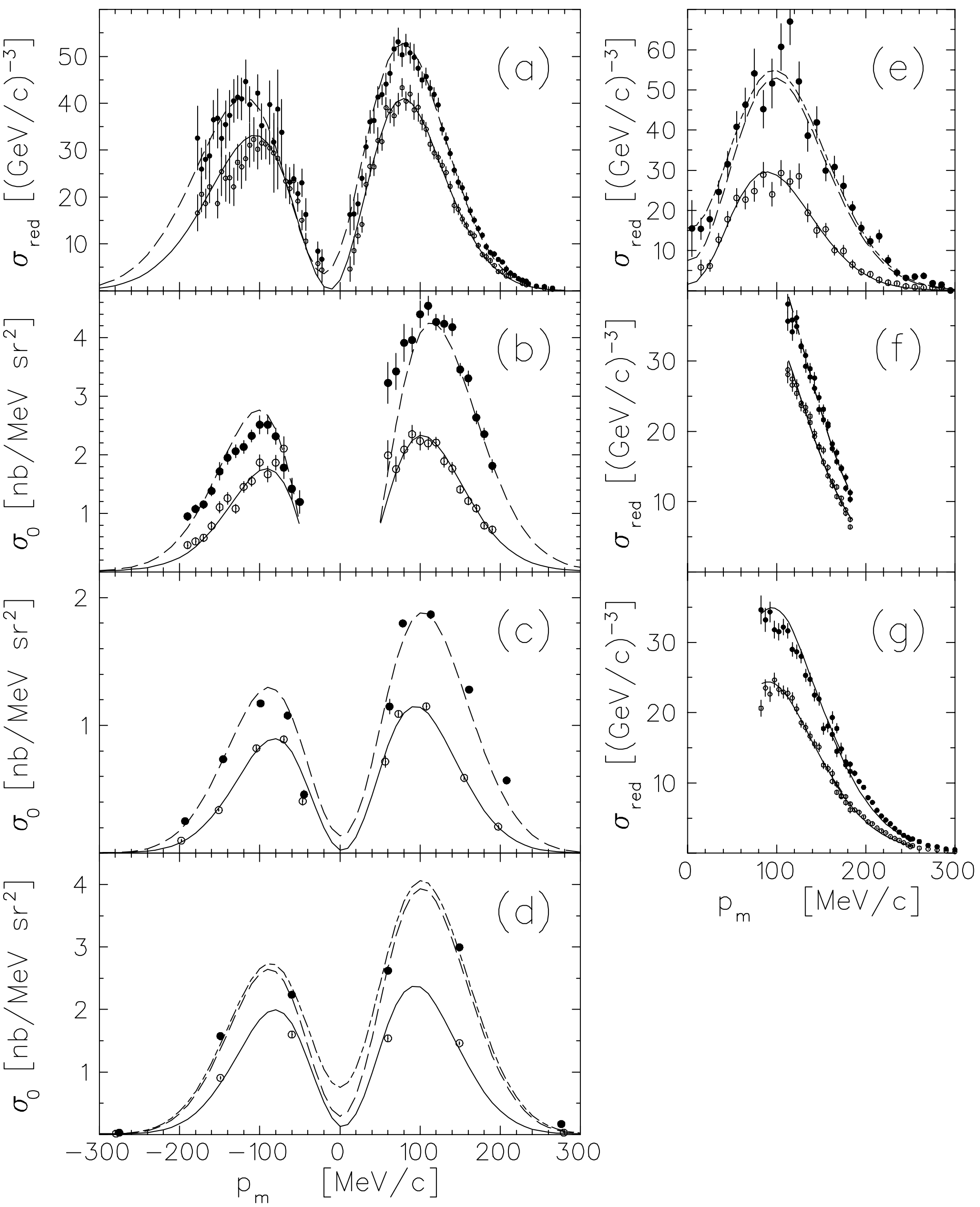

FIG. 6: Scale-factor fits to $^{16}\mathrm{O}(e,e'p)(1p)^{-1}$ data. Open points and solid lines pertain to $1p_{1/2}$, while solid points and dashed lines refer to $1p_{3/2}$. Dash-dotted lines include positive parity contributions to the 6.32 MeV peak. These fits use NLSH-P wave functions and the EDAD1 optical potential.

tested whether recent model wave functions would satisfactorily reproduce the experimental missing momentum distributions independently of Q^2. Unfortunately, neither HS, NLSH, nor NLSH-P passes this test well. From a χ^2 perspective it is clear that NLSH offers the best description at $Q^2 = 0.8$, but that most of the lower Q^2 data would prefer either NLSH-P or HS; HS may be the best compromise presently available. An estimate of the uncertainty

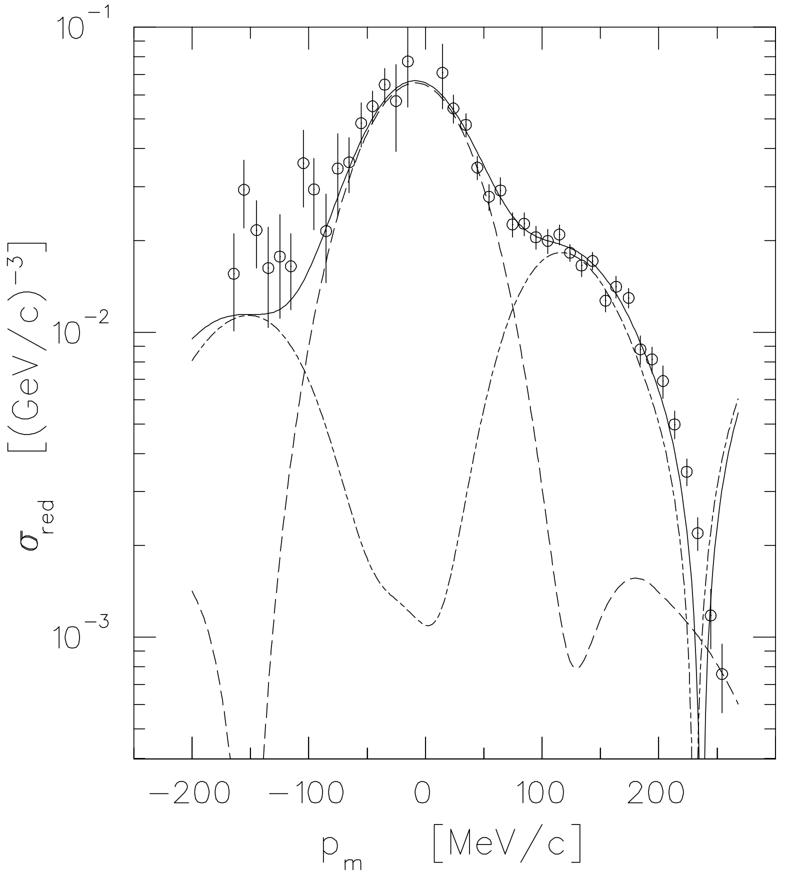

FIG. 7: Fit to Leuschner data for the positive-parity doublet at $E_m = 5.3$ MeV.

in normalization factors due to variations of the bound-state wave function can then be made by comparing NLSH/HS and NLSH-P/HS ratios for each state using the same optical potential and other model input. Thus, for the lowest $1p_{1/2}$ and $1p_{3/2}$ states we obtain ratios of approximately 1.08 and 1.02 for NLSH or 0.96 and 0.87 for NLSH-P averaged over all data sets. These ratios are qualitatively consistent with the behavior near the peaks of the momentum distributions shown in Fig. 11. Therefore, a conservative estimate of the uncertainty due to the bswf is of order $\pm 10\%$. Similarly, if we compare the two optical potentials, we find that for $Q^2 < 0.4$ the ratio between scale factors for EDAIO/EDAD1 for a given data set averages to about 0.90; the corresponding ratio becomes 0.98 at $Q^2 = 0.8$ where the attenuation in these potentials is practically identical. Therefore, the uncertainty due to variations of the optical potential is at least $\pm 5\%$ and would probably be larger if the sample of reasonable potentials were expanded.

Inspection of Table IX suggests that there would be similar uncertainties in the normalization factors for $Q^2 = 0.8$ arising from Gordon and gauge ambiguities in the single-nucleon current operator. Note that values of S_α for the same model are generally larger in Table IX than in Table VIII because the former using the entire p_m range while the latter is limited to $p_m < 200$ MeV/c where the reaction model is likely to be most accurate. Data for larger p_m also tend to increase χ^2_ν also. These problems for large p_m could arise from inaccuracy of the bswfs beyond the Fermi momentum, neglect of two-body currents, neglect of channel coupling in the final state, density-dependent form factors, etc. Therefore, a realistic estimate

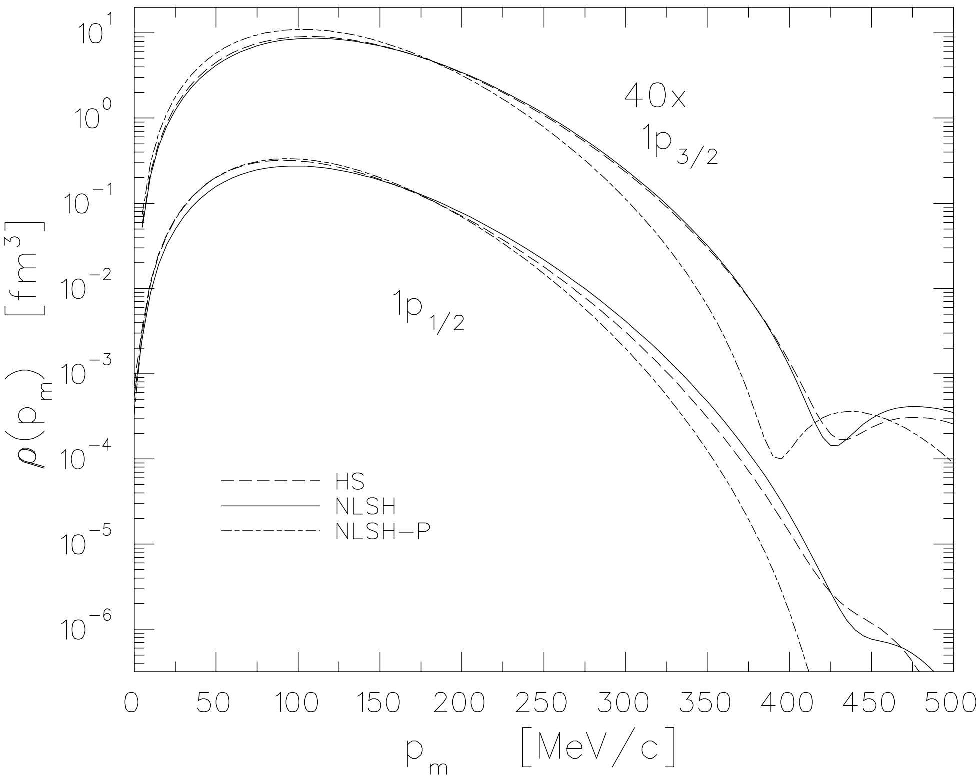

FIG. 8: Comparison between plane-wave momentum distributions for the various models.

of the model dependence of normalization factors for $(e, e'p)$ reactions should not be less than $\pm15\%$. This estimated precision is consistent with that in [2] — although the relativistic model improves our description of left-right asymmetries, recoil polarization, and other normalization-independent features of the electromagnetic knockout reaction, the model dependencies that affect the normalization uncertainty have not improved significantly in the interim. Assuming that the reaction model is most reliable at large Q^2 and modest p_m, we average all six entries in Table VIII to conclude that the spectroscopic factors for the lowest $1p_{1/2}$ and $1p_{3/2}$ states in ^{16}O are approximately 0.63(9) and 0.60(9). Note that these averages are pulled down by inclusion of NLSH-P.

To obtain more precise spectroscopic factors, it would be necessary to apply a relativistic analysis to data in quasiperpendicular kinematics for several values of Q^2 larger than about 0.5 $(\mathrm{GeV}/c)^2$ and with sufficient coverage of the p_m distribution to fit the wave function, requiring that the bswf be independent of Q^2. Although such data do not yet exist for ^{16}O, a recently completed experiment [118] will provide more complete p_m coverage for $Q^2 = 0.9$.

Lapikás *et al.* also used the bswfs and spectroscopic factors obtained from their non-relativistic analysis at low Q^2 to analyze the transparency of ^{12}C for Q^2 up to 7 $(\mathrm{GeV}/c)^2$ and the summed $1p$ and $1s$ spectroscopic amplitude. They found the summed spectroscopic strength is approximately constant at 0.58 for $Q^2 \lesssim 0.6$ $(\mathrm{GeV}/c)^2$, but rises for larger Q^2 and appears to approach the independent particle limit of unity somewhere near $Q^2 \sim 10$ $(\mathrm{GeV}/c)^2$. They speculated that the apparent Q^2 dependence of the spectroscopic strength might be related to the resolution at which a quasiparticle is probed, with long-range correlations that deplete the single-particle strength becoming less imporant at higher Q^2 and

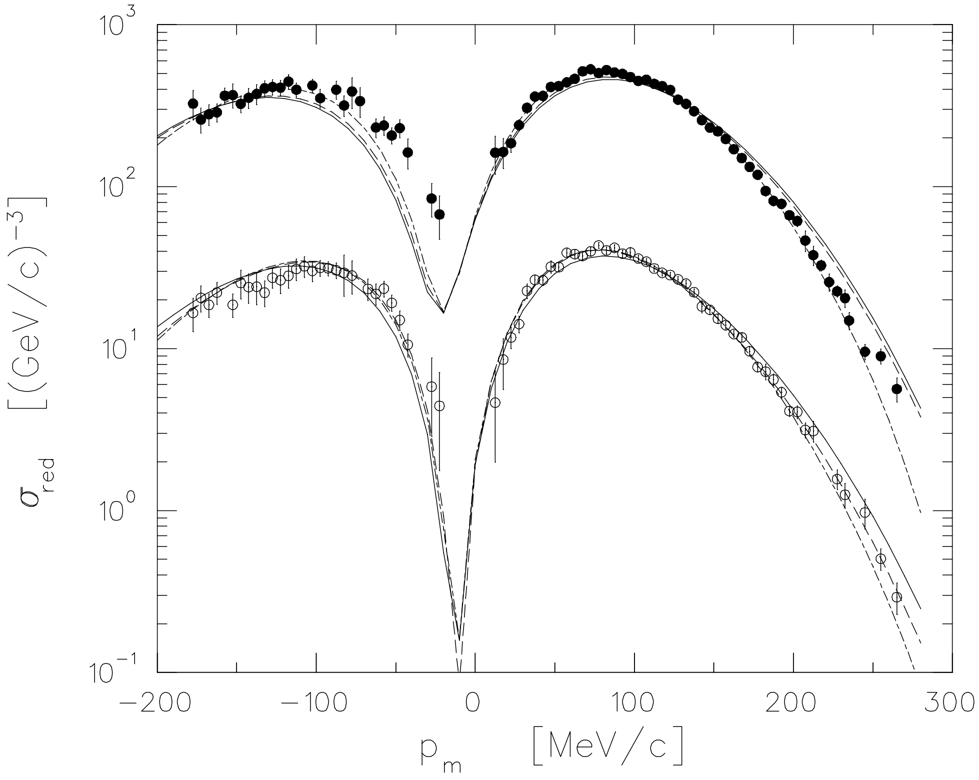

FIG. 9: Sensitivity of Leuschner data to choice of bswf, where dashed is HS, solid is NLSH, and NLSH-P is dash-dotted. Open (solid) points are for 1p1/2 (1p3/2). Data and calculations for 1p3/2 are multiplied by 10.

finer resolution. A subsequent analysis using Glauber calculations for heavier targets tends to support that interpretation [d].

We see little evidence for a systematic dependence upon either T_p or Q^2 in the normalization factors for the lowest $1p$ states of ^{16}O for the data that are currently available. Unfortunately, these data do not reach high enough Q^2 to address the resolution hypothesis. Furthermore, the normalization factors for two of the data sets appear to be anomalously low. A normalization problem might not be too surprising for data set (e) because it comes from one of the earliest experiments on this reaction, but data set (g) comes from a fairly recent experiment at Mainz and uses an ejectile energy large enough for one to expect the reaction model to be pretty reliable. As discussed above for the case of ^{12}C, we believe it likely that data set (g) has a normalization error. If we disregard these two data sets, the remaining low Q^2 data are consistent with the normalization deduced from the current $Q^2 = 0.8$ data.

[a] L. Lapikás, G. van der Steenhoven, L. Frankfurt, M. Strikman, and M. Zhalov, Phys. Rev. C 61, 064325 (2000)

[b] K. I. Blomqvist *et al.*, Z. Phys. A 351, 353 (1995)

[c] J. J. Kelly, Phys. Rev. C56, 2672 (1997)

[d] L. Frankfurt, M. Strikman, and M. Zhalov, Phys. Lett. B503, 73 (2001)

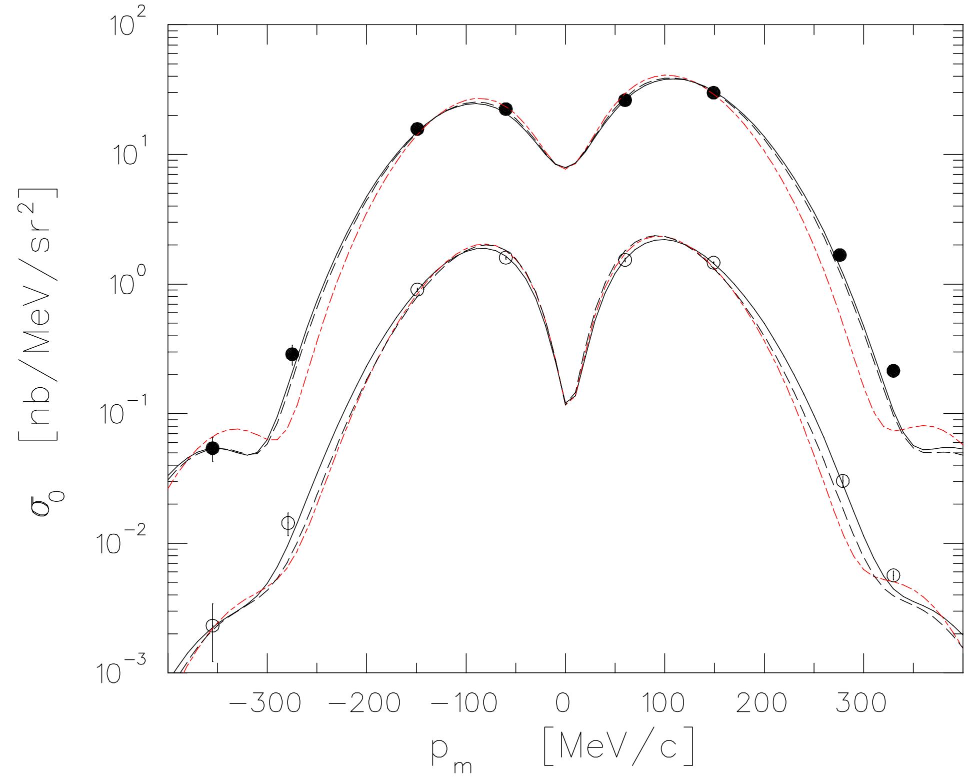

FIG. 10: Sensitivity of Gao data to choice of bswf, where dashed is HS, solid is NLSH, and NLSH-P is dash-dotted. Open (solid) points are for 1p1/2 (1p3/2). Data and calculations for 1p3/2 are multiplied by 10.

V. LEFT-RIGHT ASYMMETRY

For the sake of completeness I also compare A_{LT} for these models with the available three data sets in Fig. 11. There is very little sensitivity to the choice of bswf, whereas the Gao data show a slight preference for the EDAIO optical potential; however, this preference is not convincing because the effect is mostly at large p_m where other effects become important also.

More detailed comparisons will be made in the next update.

VI. GORDON AMBIGUITIES

The sensitivity of calculations for the Gao data to Gordon ambiguities is shown in Fig. 12. This figure uses NLSH wave functions and the EDAIO optical model, our present defaults, but I have not yet examined other combinations. Both CC2 and CC3 fit the cross section equally well, but CC1 is slightly disfavored. CC3 gives a slightly better fit for A_{LT} for $1p_{3/2}$, but CC2 seems best for $1p_{1/2}$. Unfortunately, these data do not seem to offer a clear preference. The sensitivity of A_{LT} to the Gordon ambiguity increases with p_m provided that one the one-body current remains dominant over this entire range.

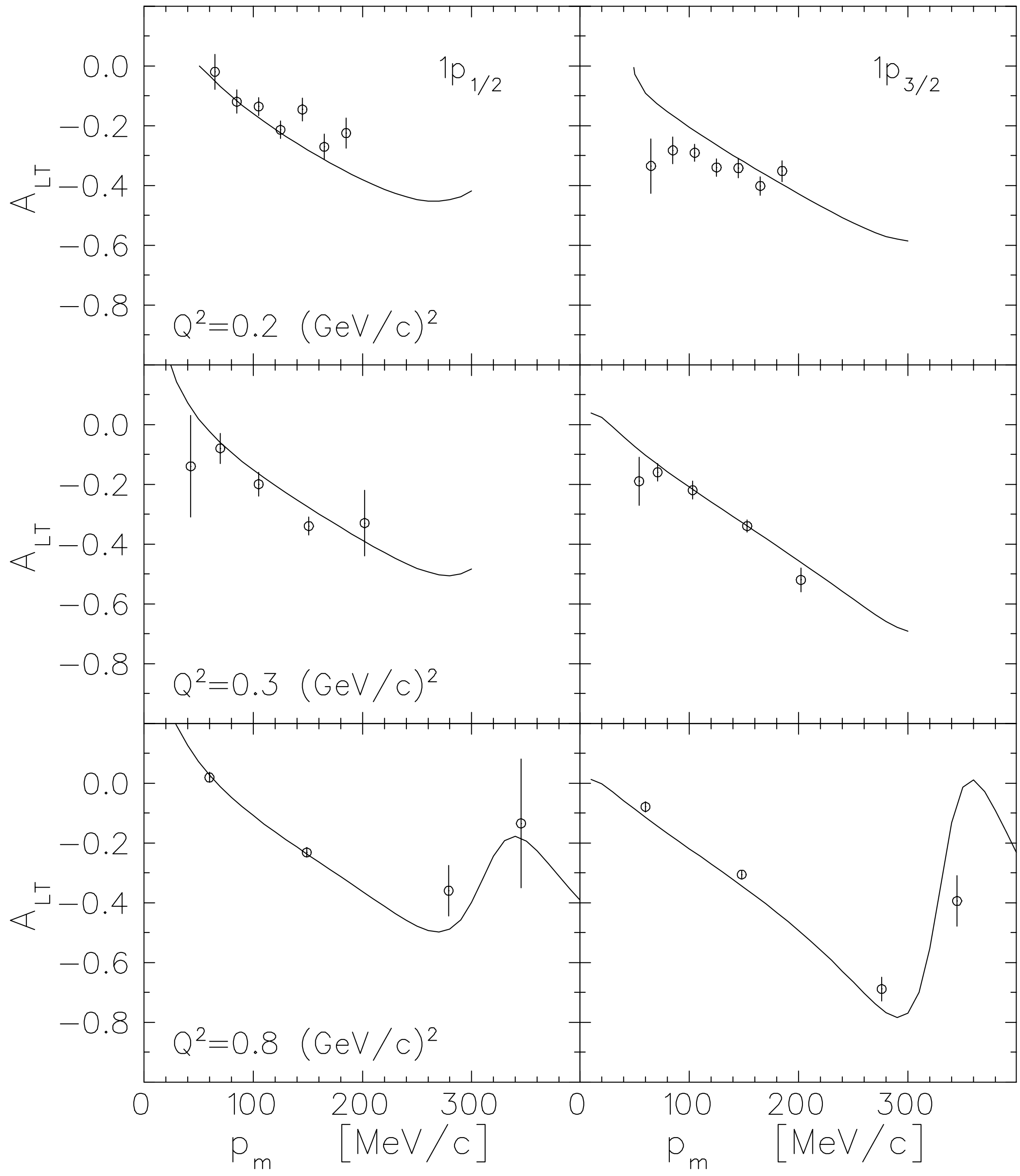

FIG. 11: A_{LT} for $^{16}\mathrm{O}(e,e'p)(1p)^{-1}$ using CC2, NLSH, EDAIO.

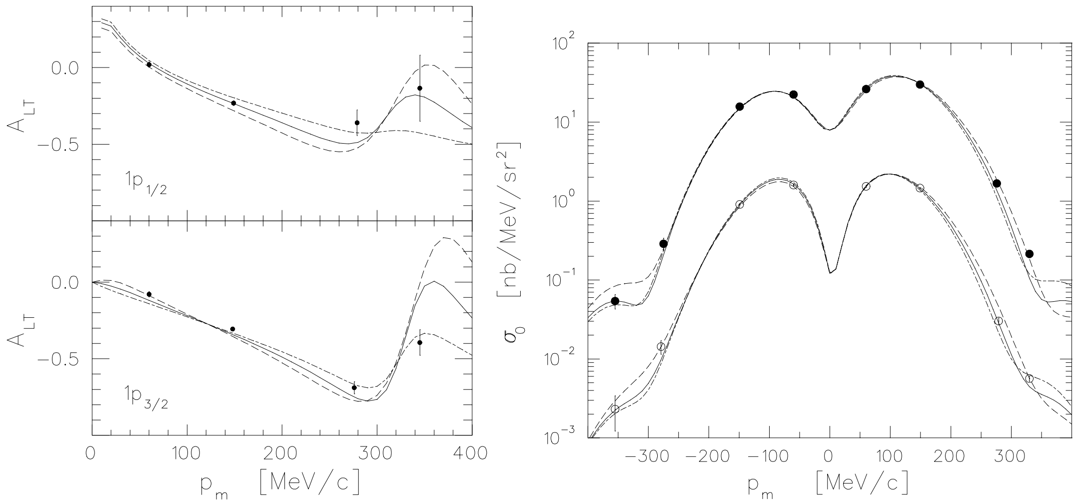

FIG. 12: Sensitivity of A_{LT} at $Q^2 = 0.8$ to Gordon ambiguity, comparing CC1 (dashed), CC2 (solid), CC3 (dash-dot) using NLSH and EDAIO.